13th International Symposium on Turbulence and Shear Flow Phenomena (TSFP13)
Montreal, Canada, June 25-28, 2024

Turbulent actuation of inlet flow for a mild adverse-pressure gradient boundary layer

Ehsan Asgari
Department of Mechanical Engineering
Dalhousie University
Halifax, NS, Canada
Ehsan.asgari@dal.ca

Mohammad Saeedi*
Department of Mechanical Engineering
Dalhousie University
Halifax, NS, Canada
mohammad.saeedi@dal.ca

ABSTRACT

In this paper, we investigate the turbulence generation for LES of a shear layer in the context of a high-order spectral-element method using upstream tripping. An arc-type trip is located near the inlet boundary of a configuration with mild adverse pressure gradient. We examine how the resulting turbulent boundary layer separates to form a shear layer. The tripping technique is compared with a previously validated precursor method in terms of computational cost, accuracy and effort. Validation is conducted using a reference experiment in terms separation and reattachment locations. Finally, we investigate the sensitivity of the generated turbulent boundary layer to the trip height and location to optimize these parameters for the application under study.

INTRODUCTION

Deterministic computation for prescribing turbulent inlet condition for scale-resolving method including direct numerical simulation (DNS) and large-eddy simulation (LES includes rescaling/recycling (Lund et al., 1998) and precursor simulation (Asgari et al., 2022), which are relatively costly and generally require an auxiliary domain. In this approach, the velocity data on a certain plane is recorded to later be fed into the main simulation as an inflow condition. An issue associated with these approaches is the so-called spurious periodicity that imposes an artificial frequency onto the recorded velocity data. This can be potentially alleviated by extending the length of the auxiliary domain to a significant multiple of the boundary layer thickness ($> 60\delta$) (Jiménez et al., 2010; Simens et al., 2009). Consequently, further additional computational cost would be imposed on the entire simulation campaign. Furthermore, a large disk storage is needed to record the instantaneous velocity field. The latter may be considered an advantage as the velocity library could be used for several simulations. However, dealing with the technical aspects of the inflow library including the convenient data format and need for temporal interpolation in case of reducing the CFL/time-step introduce more difficulties when using precursor simulations.

In recent years, there's been an interest to implement higher-order numerical schemes such as flux reconstruction (Witherden et al., 2014) and spectral element methods (SEM) (Fischer et al., 2022; Moxey et al., 2020) due to their superior accuracy and low-dissipation characteristics. Lately, (Capuano et al., 2023) compared three packages including a general purpose finite-volume method (FVM) package OpenFOAM, an SEM code Nek5000 and an immersed-boundary in-house code for a flow past a sphere. They demonstrated that for a comparable accuracy, OpenFOAM needed a significantly higher number of degrees of freedom, hence higher cost. This is a well-enough reason to opt for the high-order schemes due to their higher accuracy and reasonable cost. In case of simulation of turbulent boundary layers with SEM, owing to their low-dissipative nature, it could be more efficient to produce the inlet turbulence by means of more trivial methods such as tripping. As such, the flow disturbances behind a trip are damped less frequently and a natural transition to turbulence can be expected. However, an extended upstream length is likely necessary for the turbulence to develop. Another advantage over the traditional rescaling/recycling method is the absence of the spurious periodicity.

In this paper, we investigate the generation of turbulence for a boundary layer over a gently-curved backward facing step using a tripping method using a high-order spectral-element code Nektar++ (Moxey et al., 2020). The configuration under study is sensitive to the upstream turbulence, which makes it an ideal test case for assessment of the tripping method performance. We compare the computational cost of the tripping technique versus that of a precursor approach performed in the FVM code OpenFOAM (Weller et al., 1998). We also evaluate the accuracy of results by considering reference experimental data. The insights gained from this study will not only contribute to the validation of the tripping method but also provide valuable insights into the computational costs associated with generating turbulence in each approach.

TEST CASE AND NUMERICAL SETUP

The configuration under study is a gently curved backward facing step. The incoming flow is an incompressible turbulent boundary layer undergoing a weak adverse pressure gradient in the ramp-down region. The geometry and the boundary condition are schematically presented in Figure 1.

The test case has been investigated in an experimental study by (Zhong & Zhang, 2013). The geometrical dimensions of the domain are identical to those in numerical study of Lardeau and Leschziner (Bentaleb et al., 2012). The configuration consists of a ramp with a reference height H. A flat surface is extended $8H$ upstream the start of the ramp-down. The top boundary is located about $9.5H$ away from the origin and serves as a wall. The Reynolds number based on the ramp height and free-stream velocity (U_∞) is $Re_H \approx 13{,}700$ and the boundary layer enters the domain with a Reynolds number of $Re_\theta \approx 1{,}200$ based on the momentum thickness, with a boundary layer thickness of $\delta \approx 0.8H$. The ramp geometry can be defined via three mathematical expressions [40]:

$$Y_{wall} = (1 - 4.03H) + \sqrt{(4.03H)^2 - x^2} \;\; if \; 0 \leq x/H \leq 2.3$$

$$Y_{wall} = 1.936H - \sqrt{\frac{(4.03H)^2}{4} - (3.449H - x)^2}$$

$$if\ 2.3 \leq x/H \leq 2.835$$

$$Y_{wall} = 0.334H - \sqrt{(0.334H)^2 - (2.9365 - x)^2}$$
$$if\ 2.835 \leq x/H \leq 2.936$$

In order to actuate the incoming boundary layer and generate the desired level of turbulence, the upstream plate is further extended to $x/H = -15$ and an arc-shape turbulator is utilized to trip the boundary layer and energize the incoming flow at the inlet whose effect is under investigation in the current research.

The tensorial form of the mass and momentum conservation equations in a Cartesian coordinate system and for an incompressible flow are expressed below:

$$\frac{\partial u_i}{\partial x_i} = 0,$$
$$\frac{\partial u_i}{\partial t} + u_j \frac{\partial u_i}{\partial x_j} = -\frac{\partial p}{\partial x_i} + \nu \frac{\partial^2 u_i}{\partial x_j \partial x_j}$$

where u_i and p refer to the velocity and pressure, respectively.

The solver used in the current research (Nektar++) is a spectral h/p element code developed using C++ programming language. Spectral element computational fluid dynamics (CFD) is a powerful numerical method used to simulate fluid flow phenomena with high accuracy and efficiency. It combines elements of spectral methods and finite element methods to achieve robustness and flexibility in handling complex geometries and turbulent flows.

At its core, SEM discretizes the computational domain into a mesh of high-order elements, typically triangles or quadrilaterals in two dimensions and tetrahedra or hexahedra in three dimensions. Within each element, the solution is represented using high-order polynomial basis functions, such as Legendre or Chebyshev polynomials. These basis functions provide accurate approximation properties and enable spectral accuracy in representing the solution.

One of the key features of spectral element CFD is its ability to achieve high-order accuracy while maintaining computational efficiency. This is achieved through the use of Gauss-Lobatto-Legendre quadrature points within each element, which allows for accurate integration of the governing equations. Additionally, the use of high-order polynomials enables the representation of complex flow features with fewer degrees of freedom compared to traditional finite element or finite volume methods. It is particularly well-suited for simulating turbulent flows as in the current study, where resolving a wide range of length scales is essential. By leveraging high-order polynomial basis functions, spectral element methods can capture small-scale turbulent structures with greater fidelity compared to lower-order methods. Furthermore, the flexibility of spectral element meshes allows for adaptive refinement in regions of interest, enhancing the resolution where needed while maintaining efficiency elsewhere.

The number of planar macro-elements for SEM is approximately 7300 and a polynomial order of 4 is used. In the spanwise direction, 128 Fourier planes are distributed over a distance of $2.6H$ to yield a sufficiently fine z^+. Since there is no explicit subgrid-scale (SGS) model implemented in Nektar++, a spectral vanishing viscosity (SVV) mechanism is used to perform implicit LES for stabilizing the solution. The SVV cut-off ratio is 0.8, implying the lower 80% of frequency range is not affected by SVV. The time-step size is fixed to guarantee a CFL below 0.4 and a second-order temporal scheme (IMEX2) is employed to advance the solution in each time-step.

An important part in a scale-resolved CFD simulation is the mesh generation. SEM generally requires coarse macro-elements that will be utilized to form intra-element quadrature points. The "*h*/*p*" designation is usually applied to such methods to imply a two-folded approach towards grid resolution. The "*h*" refers to macro-element size which is commonly used in linear meshes generated for finite-volume codes. On the other hand, "*p*" indicates the order of polynomials utilized to approximate the velocity inside a single macro-element. As mentioned before, a polynomial order of 4 is used in the current study. Nevertheless, a good-quality mesh is beneficial for resolving the boundary layer in the current study. A common issue usually faced in the high-order methods including SEM, is generating a coarse mesh for curved boundaries. The coarse mesh has to somehow store extra information to represent the boundary curvature with a reasonable accuracy, as it is essential to have a smooth boundary when polynomial order is increased. In other words, a coarse mesh (low "*h*") is necessary as the first step to construct high polynomial order (increased "*p*"). We have applied this approach through a block-structured methodology using the package, GridPro. More specifically, we implemented a cubic mesh output, such that the high-resolution linear mesh is divided by 3×3 to yield the coarse mesh while keeping the initial information for high-order reconstruction of the curved boundaries.

RESULTS

The three-dimensional turbulent structures of the boundary layer are demonstrated using iso-surfaces of Q criterion in Figure 2. As seen, the tripping method, if applied with suitable parameters, can efficiently trigger transition to turbulence. It is observed that in the post-separation region, the flow structures grow in size and form a thicker turbulent boundary layer.

To assess the role of trip height and position, we consider 4 cases. The base case (T1) consists of an arc-trip located at $x/H = -14.5$ with a height of $0.0625H$. The arc-trip is fraction of a cylinder with the radius of $0.125H$. The trip configurations and their specifications are presented in Table 1. Case T4 is considered to evaluate the effect of trip location by positioning the trip further downstream. The other configurations only differ in the trip height as seen in Table 1.

Table 1 Configuration with different trip height or location.

Case	*Location*	*Height*
T1	$x/H = -14.5$	$0.0625H$
T2	$x/H = -14.5$	$0.0225H$
T3	$x/H = -14.5$	$0.125H$
T4	$x/H = -10.5$	$0.0625H$

In all cases, a power-law velocity profile has been prescribed at the inlet as:

$$u = U_\infty(\frac{y-H}{\delta})^n,$$

where δ represents the boundary layer thickness at the inlet. The power n was tested with values ranging from $\frac{1}{7}$ to $\frac{1}{11}$ and the value $\frac{1}{11}$ was selected for a smoother velocity profile.

In Figure 3 the instantaneous streamwise velocity contours for the developing boundary layer with presence of the prescribed trips are qualitatively shown for cases T1, T2, T3, and T4, respectively. As is qualitatively observed from the velocity contours, only cases T1 and T3 have made the flow highly turbulent and separated wake flow behind the trips energizes the boundary layer and creates sustained turbulence level downstream, while T2 is unable to actuate the non-perturbed flow. Interestingly, the boundary layer behind the trip in T4 eventually transitioned to turbulence in the far downstream. It is noted that T1 and T4 have identical trip shapes but differ in the trip position. This may arise a question as to why this difference is observed between these two cases. To elucidate the source of it, we have considered another simulation with T1 configuration but with a Blasius velocity profile imposed with the same boundary layer thickness. The instantaneous velocity profile of this special case is presented in Figure 4. As observed, there is no turbulence formation behind the trip. It is therefore deduced that aside from the trip height, the inlet profile shear rate plays an important role in transitioning to turbulence.

A comparison between the resulted locations of separation and reattachment points (which are qualitatively shown in Figure **5**) using different approaches and configurations compared with the reference experimental data of (Zhang & Zhong, 2011) are presented in Table 2. It is seen that the maximum relative error for the no treatment case is 70% which drops to 22% for the precursor simulation and 4% for the tripping configuration T1 which indicates the acceptable accuracy of the tripping method for the first-order time-averaged statistics. It is however noted that the other tripping configurations have yielded lower relative errors compared to the precursor case, except T2 that was unable to generate turbulence and hence a performance similar to no-trip case.

Table 2 Comparison between separation and reattachment locations.

Case	*Sep.*	*Reattach.*	*Rel. err.*
Exp.	$x/H = 1.09$	$x/H = 4.21$	-
precursor	$x/H = 0.79$	$x/H = 4.6$	22%
T1	$x/H = 1.01$	$x/H = 4.05$	4%
T2	$x/H = 0.55$	$x/H = 6.86$	63%
T3	$x/H = 1.1$	$x/H = 3.8$	10%
T4	$x/H = 0.99$	$x/H = 4.54$	8%
no trip	$x/H = 0.58$	$x/H = 5.9$	70%

According to Figure 5, various trip configurations have resulted in different thicknesses of mean separated bubbles. As seen, the thickness correlates with the reattachment locations that are marked by a circle.

Evolutions of vertical profiles of the time-averaged streamwise velocity are provided in Figure 6. It is observed that in absence of an inflow actuation (no-trip), the profiles and the flow field shown previously in Figure 5 significantly deviate from the experimental measured data indicating the sensitivity of the test case to the inlet turbulence. It is seen that among the tripping cases, T1 and T4 match best with the reference experiment. T2 expectedly is not providing an accurate prediction and has deviated from other tripping cases. T3 has resulted in profiles with more discrepancy compared to T1. In general, however, both precursor simulation and tripping method significantly improve the agreement of the first-order statistics with the experimental data.

Evolution of normal Reynolds stress normal component $\langle u'u' \rangle$ as the main contributor to the turbulent kinetic energy is exhibited in Figure 7 at same location as of the mean velocity profiles. It is observed that T1 and T3 have resulted in profiles very close to the experiment data. On the other hand, T4 has mostly overpredicted the Reynolds stress. Further, T2 is observed to postpone transition to turbulence in the separated bubble region, as the level of Reynolds stress is far lower than the other cases.

In terms of computational cost, we have compared the normalized wall-time required for each approach in Table 3. Accordingly, it is clearly demonstrated that the used tripping method is computationally more affordable and more feasible in comparison with the precursor technique since the latter practically entails two simulations, one for generating the inflow data in the so-called auxiliary domain, and one for the main computational domain. Also, since the auxiliary domain should be sufficiently long to alleviate the spurious periodicity it imposes substantial computational cost. Other factors to add are data handling and formatting the generated data.

Table 3 Comparison between computational cost of each approach.

Method	*Computational time*
trip	1
precursor	2.5-3

CONCLUSIONS

As discussed above, precursor simulation approach for generating inlet turbulence is a computationally expensive method. It consists of two simulations: an auxiliary and a primary simulation. The auxiliary simulation is significantly expensive, for it demands a very long domain to represent a developing turbulent boundary layer on a flat plate. Typically, a substantial time is spent to first adjust the inlet conditions such as the boundary layer or the momentum thickness, and second to run the simulation for a very long time to record the velocity data on a certain plane. The plane position should be selected based on the target conditions: boundary layer or momentum thickness of the primary domain. The point is that locating the plane also comes with trial and errors. Also, it is very common for the auxiliary domain to be much longer than the primary domain, to mitigate the influence of spurious periodicity (Asgari & Saeedi, 2024). There are other costs associated with the precursor approach, including storage, handling, formatting and scaling if necessary. The size of generated data is quite huge and satisfying these requirements are not straightforward.

The tripping approach that was proposed and discussed in this paper eliminates the need for an auxiliary domain, at the cost of increasing the primary domain length. However, we

demonstrated that the associated cost is negligible compared to the precursor approach.

In addition, our findings indicate that the choice of inlet velocity profile significantly influences the flow transition process to turbulence. The selection of an appropriate velocity profile tailored to the specific flow conditions and desired turbulence characteristics might be critical for achieving accurate and reliable results. Further investigation into the sensitivity of the flow transition process to different inlet velocity profiles will contribute to the application of the tripping method in practical simulations.

Moreover, the effectiveness of the tripping method may vary depending on the specific flow configuration and boundary conditions. Therefore, a systematic parametric study is deemed to be essential to understand the optimal conditions for its application. Additionally, it is crucial to assess the scalability and robustness of the tripping approach across different flow regimes and geometries. These future topics will provide valuable insights into the practical implementation of the tripping method for generating inlet turbulence in scale-resolving simulations. Hence, further investigation is required to evaluate these details and merits of the tripping method that will be realized in the future.

REFERENCES

Asgari, E. & Saeedi, M. (2024). The Influence of Spurious Periodicity on the Flow Characteristics of a Separated Turbulent Boundary Layer with and Without Active Flow Control. *Flow, Turbulence and Combustion*, 1–24.

Asgari, E., Saeedi, M. & Etemadi, M. (2022). Large-eddy simulation of a developing turbulent boundary layer over a wall-mounted hemisphere under the influence of a surrounding ditch: Flow characteristics and aerodynamic forces. *Journal of Wind Engineering and Industrial Aerodynamics*, *227*, 105047.

Bentaleb, Y., Lardeau, S. & Leschziner, M. A. (2012). Large-eddy simulation of turbulent boundary layer separation from a rounded step. *Journal of Turbulence*, *13*, N4.

Capuano, F., Beratlis, N., Zhang, F., Peet, Y., Squires, K. & Balaras, E. (2023). Cost vs Accuracy: DNS of turbulent flow over a sphere using structured immersed-boundary, unstructured finite-volume, and spectral-element methods. *European Journal of Mechanics-B/Fluids*, *102*, 91–102.

Fischer, P., Kerkemeier, S., Min, M., Lan, Y.-H., Phillips, M., Rathnayake, T., Merzari, E., Tomboulides, A., Karakus, A., Chalmers, N. & others. (2022). NekRS, a GPU-accelerated spectral element Navier-Stokes solver. *Parallel Computing*, *114*, 102982.

Jiménez, J., Hoyas, S., Simens, M. P. & Mizuno, Y. (2010). Turbulent boundary layers and channels at moderate Reynolds numbers. *Journal of Fluid Mechanics*, *657*, 335–360.

Lund, T. S., Wu, X. & Squires, K. D. (1998). Generation of turbulent inflow data for spatially-developing boundary layer simulations. *Journal of Computational Physics*, *140*(2), 233–258.

Moxey, D., Cantwell, C. D., Bao, Y., Cassinelli, A., Castiglioni, G., Chun, S., Juda, E., Kazemi, E., Lackhove, K., Marcon, J. & others. (2020). Nektar++: Enhancing the capability and application of high-fidelity spectral/hp element methods. *Computer Physics Communications*, *249*, 107110.

Simens, M. P., Jiménez, J., Hoyas, S. & Mizuno, Y. (2009). A high-resolution code for turbulent boundary layers. *Journal of Computational Physics*, *228*(11), 4218–4231.

Weller, H. G., Tabor, G., Jasak, H. & Fureby, C. (1998). A tensorial approach to computational continuum mechanics using object-oriented techniques. *Computers in Physics*, *12*(6), 620–631.

Witherden, F. D., Farrington, A. M. & Vincent, P. E. (2014). PyFR: An open source framework for solving advection-diffusion type problems on streaming architectures using the flux reconstruction approach. *Computer Physics Communications*, *185*(11), 3028–3040.

Zhang, S. & Zhong, S. (2011). Turbulent flow separation control over a two-dimensional ramp using synthetic jets. *AIAA Journal*, *49*(12), 2637–2649.

Zhong, S. & Zhang, S. (2013). Further Examination of the Mechanism of Round Synthetic Jets in Delaying Turbulent Flow Separation. *Flow, Turbulence and Combustion*, *91*(1), 177–208.

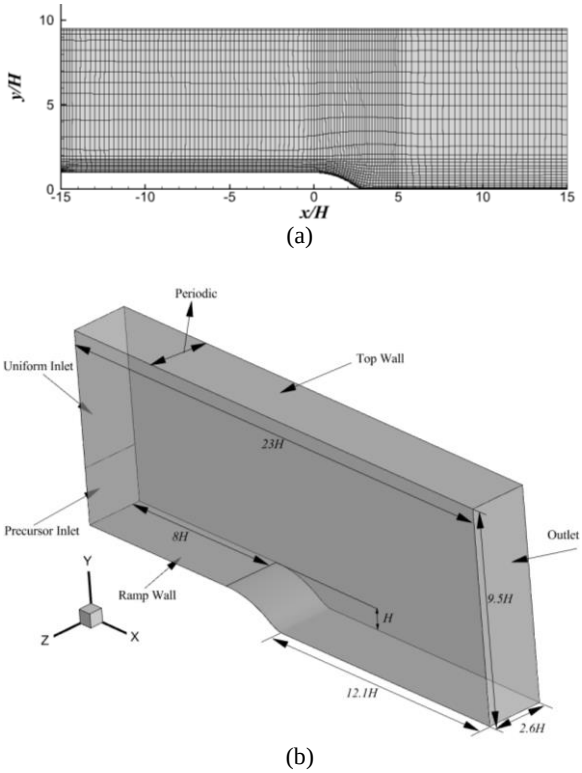

Figure 1 Planar macro-elements used for tripping method in Nektar++ with an extended upstream plate (a), three-dimensional domain with a short upstream length used for precursor approach in OpenFOAM (b).

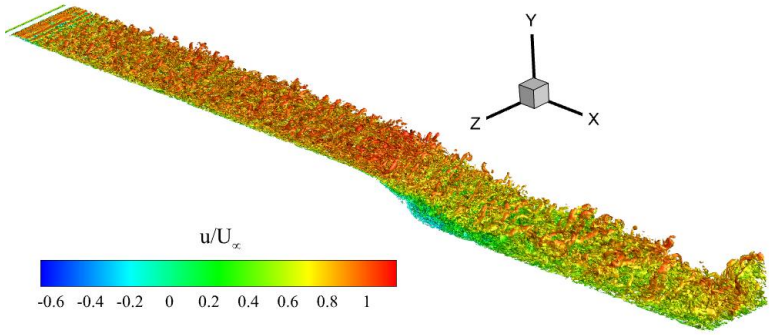

Figure 2 Three-dimensional representation of turbulent structures generated by a trip visualized by Q criterion.

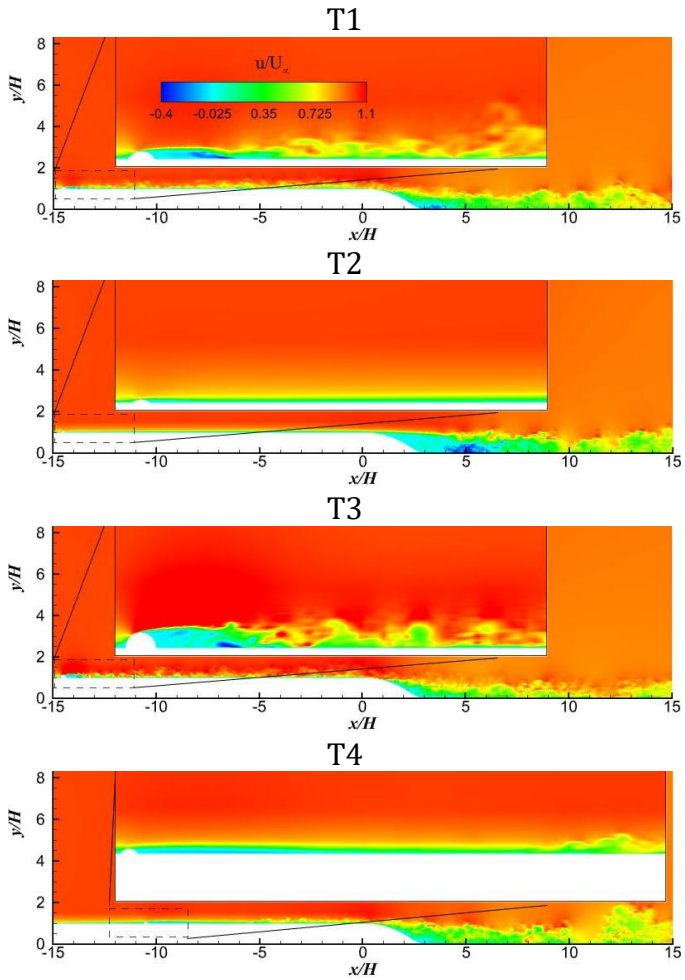

Figure 3 Instantaneous streamwise velocity of tripping cases with the magnified view behind the trip.

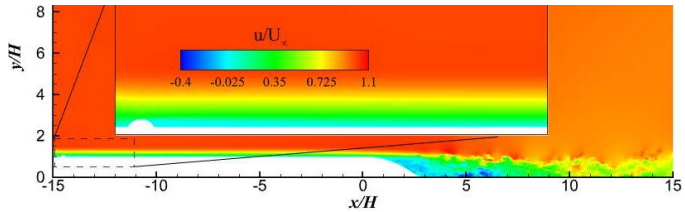

Figure 4 Instantaneous streamwise velocity of case T1 with a Blasius velocity profile at the inlet.

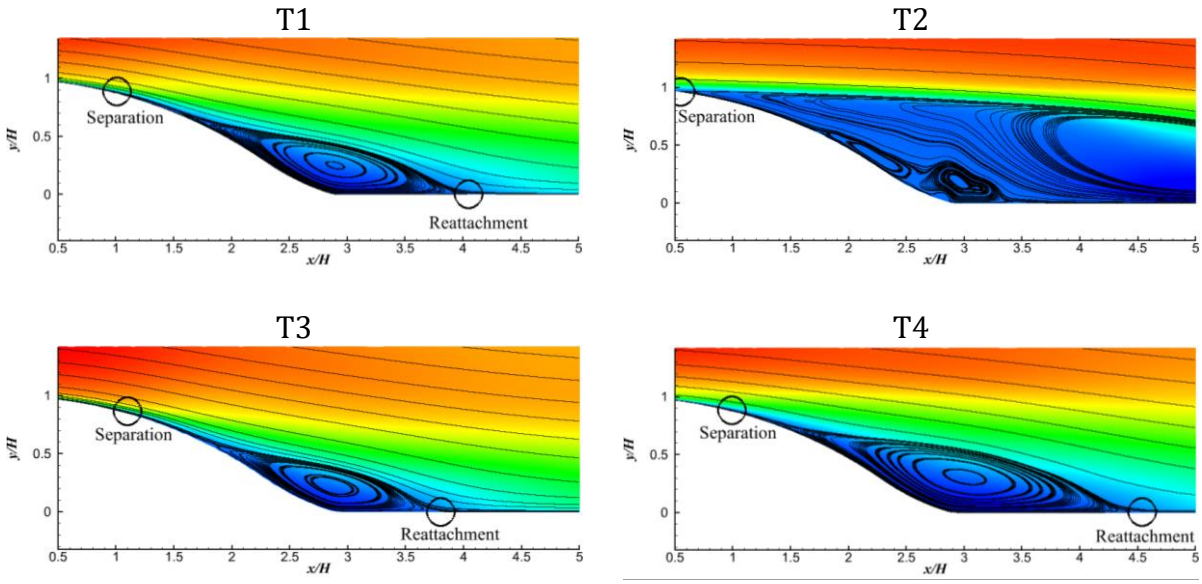

Figure 5 Mean separated bubble region visualized by mean streamlines in trip configurations.

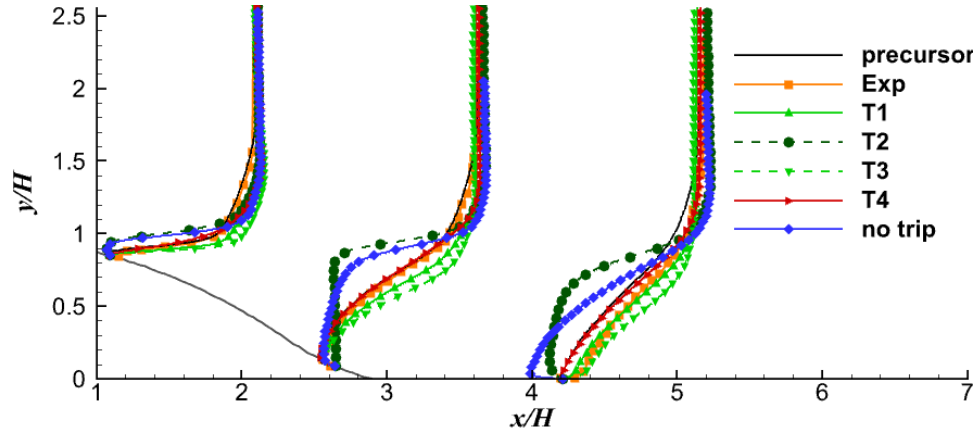

Figure 6 Evolution of time-averaged streamwise velocity for different methods and trip configurations over the ramp-down region.

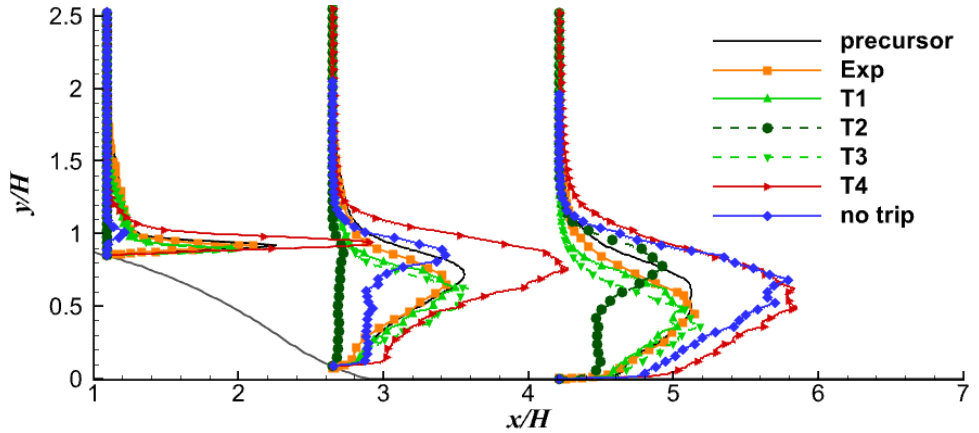

Figure 7 Evolution of normal Reynolds stress $\langle u'u' \rangle$ for different methods and trip configurations over the ramp-down region.